Acta Crystallographica Section F
Structural Biology and Crystallization Communications
ISSN 1744-3091

Expression, crystallization and X-ray data collection from microcrystals of the extracellular domain of the human inhibitory receptor expressed on myeloid cells IREM-1

Nazzareno Dimasi,[a]* David Flot,[b] Florine Dupeux[b] and José A. Márquez[b]*

[a]Istituto Giannina Gaslini, Largo Gerolamo Gaslini 5, 16147 Genova, Italy, and [b]European Molecular Biology Laboratory, Grenoble Outstation, Polygon Scientifique, 6 Rue Jules Horowitz, 38000 Grenoble, France

Correspondence e-mail: ndimasi@gmail.com, marquez@embl.fr

Received 14 November 2006
Accepted 30 January 2007

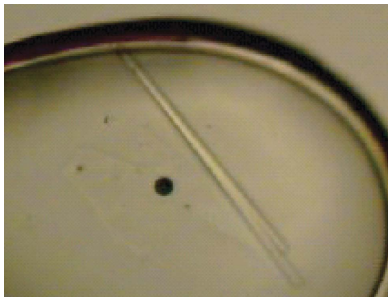

IREM-1 is an inhibitory receptor involved in the functional regulation of myeloid cells. The expression, *in vitro* folding, purification, crystallization and X-ray data collection of the Ig-V like domain of IREM-1 are reported. X-ray data were collected from a microcrystal (300 × 10 × 10 µm) at 100 K and a diffraction pattern was obtained to 2.6 Å resolution on microfocus beamline ID23-2 at the ESRF. The crystal belongs to space group $P3_121$, with unit-cell parameters $a = b = 54.23$, $c = 72.02$ Å, $\alpha = \gamma = 90$, $\beta = 120^\circ$. Assuming the presence of one molecule per asymmetric unit, V_M (the Matthews coefficient) was calculated to be 1.96 Å^3 Da^{-1} and the solvent content was estimated to be 37.27%. Determination of the IREM-1 structure will provide insights into its structural requirements for ligand discrimination and binding.

1. Introduction

The function of the leukocyte is regulated by a precise balance between positive and negative signals delivered by activating or inhibitory receptors. These signals allow leucocytes to discriminate between normal cells and invading pathogens such as parasites, bacteria and viruses. Inhibitory and activating receptors expressed on the surface of leucocytes are responsible for target recognition.

In structural terms, inhibitory and activating receptors belong to two different structural folds: the immunoglobulin-like fold and the C-type lectin-like fold (Natarajan *et al.*, 2002; Dimasi & Biassoni, 2005). Both classes contain inhibitory and activating receptors. A marked difference between inhibitory and activating receptors is the fact that inhibitory receptors are capable of directly delivering their intracellular signals (Ravetch & Lanier, 2000), while activating receptors lack any intracellular signalling domain and in order to deliver their signals need to associate with specialized signalling transduction polypeptides (Humphrey *et al.*, 2005).

Several single-domain immunoglobulin-like receptors have been identified in myeloid cells, which are the major cellular component of the innate immune system (Colonna *et al.*, 1997; Fujioka *et al.*, 1996; Chung *et al.*, 2003; Clark *et al.*, 2000; Green *et al.*, 1998; Cantoni *et al.*, 1999; Alvarez-Errico *et al.*, 2004; Aguilar *et al.*, 2004; Martinez-Barriocanal & Sayos, 2006; Allcock *et al.*, 2003; Bouchon *et al.*, 2000; van den Berg *et al.*, 2004; Pandey & Agrawal, 2006; Dietrich *et al.*, 2000). This class of receptors map on human chromosome 17 (17q25.1) and are believed to be important for the regulation of the myeloid cell function.

Of special interest are the recently identified IREM receptors, because they may have important immunoregulatory functions in controlling inflammation (Speckman *et al.*, 2003). Therefore, these receptors are attractive targets for the development of small-molecule therapeutics. Three distinct IREM receptors have recently been identified in humans: IREM-1 (Alvarez-Errico *et al.*, 2004), IREM-2 (Aguilar *et al.*, 2004) and IREM-3 (Martinez-Barriocanal & Sayos, 2006). IREM-1 is an inhibitory receptor, whereas IREM-2 and IREM-3 are activating receptors. These receptors are composed of a single extracellular immunoglobulin-like domain, a transmembrane domain and a cytoplasmic tail. The ligands recognized by this class of immune receptors are still elusive and their identification is an active area of research.

We have previously determined the solution structure of the inhibitory receptor IRp60, which was one of the first immunoreceptors to be identified on locus 17q25.1 (Dimasi *et al.*, 2007). In order to understand the structural basis of the activity of this class of immunoreceptors and to gain insight into the structural requirements for ligand discrimination and binding, we present here the expression, refolding, crystallization and X-ray data collection of IREM-1.

2. Experimental

2.1. Cloning, expression, refolding and purification

The DNA coding sequence for the immunoglobulin-like domain of human IREM-1 (NCBI entry code AAP57942), corresponding to amino acids 21–140, was constructed using 26 chemically synthesized overlapping oligonucleotides.

R0	GCCCTCCATATGGAATTCC
F0	GGAATTCCATATGGAGGGCAGCCACCATCACCATC
R19	TACCTTCAATACTTCCATGGTGATGGTGATGGTGGCT
F35	ACCATGGAAGTATTGAAGGTAGAGGAATCCCACAAATTACA
R56	TAACGGTCGTTGGCCCTGTAATTTGTGGGATTCCTC
F76	GGGCCAACGACCGTTAATGGACTAGAACGAGGTTC
R92	ACACTGGACAGTCAGGGAACCTCGTTCTAGTCCAT
F111	CCTGACTGTCCAGTGTGTGTATAGAAGCGGGTGG
R127	ACCACCATTTGAGATAAGTTTCCCACCCGCTTCTATACAC
F145	GAAACTTATCTCAAATGGTGGTGCAGGGGAGCGATATG
R167	ACTAATATCTTACAGTCACGCCATATCGCTCCCCTGC
F183	GCGTGACTGTAAGATATTAGTGAAAACTAGTGGCTCAGAG
R204	TCCCTCTTGACTTCCTGCTCTGAGCCACTAGTTTTC
F223	CAGGAAGTCAAGAGGGATCGGGTTTCAATTAAGGAC
R240	AATGTGCGATTTTTTTGGTTGTCCTTAATTGAAACCCGA
F259	AACCAAAAAAATCGCACATTTACTGTGACAATGGAAGATTT
R279	CTGCGTCCGTTTTCATCAAATCTTCCATTGTCACAGTA
F300	GATGAAAACGGACGCAGATACATACTGGTGCGGC
R317	CGTTACCGGTCTTCTCTATGCCGCACCAGTATGTAT
F334	ATAGAGAAGACCGGTAACGATCTTGGGGTAACCGTT
R353	GGGGTCGATCGTTACTTGAACGGTTACCCCAAGAT
F370	CAAGTAACGATCGACCCCGCTCCGGTAACCCAGG
R388	AGACGAAGACGTCTCCTCCTGGGTTACCGGAGC
F404	AGGAGACGTCTTCGTCTCCTACATAAGGATCCGCG
R421	GTTTCCCTCTCGTCGCCGCGGATCCTTATGTAGG
R439	GCGACGAGAGGGAAAC

Oligonuleotide F0 incorporates a start codon and an *Nde*I restriction-enzyme site, while oligonucleotide R421 includes a termination codon and a *Bam*HI site. The construct was designed to have a histidine tag at the N-terminus to facilitate protein purification, followed by a thrombin cleavage site to cut off the histidine tag from the final purified protein. The IREM-1 gene was assembled from a single mixture of all 26 oligonucleotides by 30 cycles of recursive PCR (denaturation at 367 K for 1 min, annealing to 305 K for 5 min and extension at 345 K for 1 min). The PCR product was digested with *Nde*I and *Bam*HI, purified by agarose gel electrophoresis and cloned immediately after the T7 promoter of the expression vector pT7-7. The fidelity of the construct was confirmed by DNA sequencing. With this construct, after thrombin cleavage only four amino acids, arginine, glycine, isoleucine and proline, are incorporated into the N-terminus of the IREM-1 extracellular domain (which starts with amino acid 21, glutamine of the IREM-1 sequence).

The resulting plasmid, pT7-IREM1, was transformed into *Escherichia coli* strain BL21-CodonPlus (DE3) pLysS (Stratagene). Cells were grown in Luria–Bertani medium at 310 K supplemented with 25 µg ml^{-1} ampicillin and 15 µg ml^{-1} chloramphenicol to an absorbance of 0.6 at 600 nm and were induced for 3 h with 1 m*M* isopropyl *β*-D-thiogalactoside. The cells were then harvested by centrifugation and resuspended in 100 m*M* Tris–HCl pH 8.0, 2 m*M* EDTA, 10 m*M* DTT and lysed using ultrasound sonication. IREM-1 was obtained as inclusion bodies. These were washed four times with 50 m*M* Tris–HCl pH 8.0, 0.5%(*v*/*v*) Triton X-100, 100 m*M* NaCl, 1 m*M* EDTA, 1 m*M* DTT, once with the same buffer plus 2 *M* urea and finally solubilized in 100 m*M* Tris–HCl pH 8.0, 8 *M* urea, 10 m*M* EDTA, 0.1 m*M* DTT. Insoluble material was removed by ultracentrifugation. Urea-solubilized IREM-1 was folded *in vitro* at 277 K by slow dilution to a final concentration of 5 µg ml^{-1} in 1 l 0.6 *M* arginine, 100 m*M* Tris–HCl pH 8.0, 2 m*M* EDTA, 5 m*M* reduced glutathione and 0.5 m*M* oxidized glutathione. After 48 h, the folding mixture was concentrated to a volume of 30 ml and dialyzed at 277 K against 25 m*M* Tris–HCl pH 8.0, 500 m*M* NaCl, 5 m*M* imidazole. Properly folded material was separated from aggregates by ultracentrifugation at 55 000*g* followed by 0.22 µm filtration.

The refolded protein was purified by standard metal-affinity chromatography. The N-terminal histidine tag was removed by overnight incubation at 295 K with thrombin protease (GE Healthcare). The thrombin protease was removed using a Benzamidine Sepharose column (GE Healthcare) and any uncleaved protein was removed by metal-affinity chromatography. The protein was then purified by size-exclusion chromatography using a Superdex 75 HR 10/30 column (GE Healthcare) equilibrated in 20 m*M* Tris–HCl pH 8.0, 150 m*M* NaCl. IREM-1 elutes from the gel-filtration column as a single monomeric peak with the expected molecular weight (∼15 600 Da). Mass spectrometry and N-terminal sequence analyses confirmed the identity of the protein (data not shown).

The protein concentration was measured by absorbance at 280 nm using a calculated extinction coefficient of 32 220 M^{-1} cm^{-1}. The protein was concentrated to 34 mg ml^{-1} using a 5K MWCO concentrator (Millipore), filtered using a 0.22 µm centrifuge filter, flash-frozen in liquid nitrogen and used for high-throughput crystallization screenings.

2.2. Crystal growth, data collection and processing

The initial crystallization screening was carried out at the High Throughput Crystallization Laboratory (HTX Lab.) of the EMBL Grenoble Outstation. Nanovolume crystallization experiments were performed using a Cartesian PixSys 4200 (Genomic Solutions) robot. Sitting-drop vapour-diffusion experiments were set up in Grenier Crystal Quick plates using 100 nl sample (IREM-1 at 5 or 38 mg ml^{-1} in 20 m*M* Tris–HCl pH 8.0, 150 m*M* NaCl) and 100 nl crystallization solution, equilibrating against 88 µl crystallization solution at 293 K. A total of 768 different crystallization conditions from commercially available screens were tested, including Crystal Screens I and II, Crystal Screen Lite, PEG/Ion, MembFac, Natrix, Quick Screen, Grid Screens Ammonium Sulfate, Malonate, PEG 6000, PEG/LiCl and MPD (all from Hampton Research), JCSG+ and PACT screens (from Nextal), and a 24-condition custom-made grid screen that assays formate (from 0.8 to 3.2 *M* in 0.8 *M* unit increments) against pH (from 4.0 to 9.0 in one-unit increments). Short (about 40 µm in length) needle-shaped crystals grew in condition No. 81 of the Nextal JCSG+ screen (Quiagen) after 2 d. Initial refinement experiments were performed using nanovolume drops (as described above) with the same sample and varying concentrations of PEG MME 2000 and potassium thiocyanate. Long needle-shaped crystals were obtained in 0.25 *M* potassium thiocyanate, 25%(*w*/*v*) PEG MME 2000 over a

Table 1
X-ray data-collection statistics for IREM-1 IgV-like domain.

Values in parentheses are for the highest resolution shell.

Source	ID23-2 beamline, ESRF
Wavelength (Å)	0.873
Temperature (K)	100
Space group	$P3_121$
Unit-cell parameters (Å, °)	$a = b = 54.23$, $c = 72.01$, $\alpha = \beta = 90$, $\gamma = 120$

	Merged	Data set 1	Data set 2	Data set 3	Data set 4
No. of frames	90	20	33	30	7
Resolution (Å)	19.67–2.60	19.67–2.60	19.67–2.60	19.67–2.61	19.67–2.61
No. of observations	19419	4506	7453	6570	1479
Unique reflections	3936	2686	2783	2984	1265
Data completeness (%)	97.7 (95.7)†	65.1 (65.3)‡	68.7 (66.9)‡	76.9 (80.6)§	31.3 (29.4)§
$\langle I/\sigma(I)\rangle$	9.67 (3.2)†	6.02 (2.9)‡	7.04 (2.9)‡	7.34 (3.1)§	3.96 (2.2)§
$R_{\rm merge}$¶ (%)	14.2 (38.8)†	12.5 (25.4)‡	19.3 (47.6)‡	16.1 (42.1)§	19.1 (38.6)§

Molecules per asymmetric unit	1
Crystal solvent content	37.27

† Higher resolution shell 2.60–2.70 Å. ‡ Higher resolution shell 2.60–2.76 Å. § Higher resolution shell 2.61–2.76 Å. ¶ $R_{\rm merge} = \sum_h \sum_i |I_{hi} - \langle I_h\rangle| / \sum_h \sum_i I_{hi}$, where I_{hi} is the intensity of an individual reflection.

period of 5 d and with approximate dimensions of 300 × 10 × 10 µm. Despite further efforts using both nanovolume and traditional crystallization experiments in Linbro-type plates, we did not succeed in improving the crystal size and morphology. Therefore, we proceeded with X-ray data collection.

Owing to the small crystal size, data collection was carried out at the ID23-2 microfocus beamline of the European Synchrotron Radiation Facility (ESRF), which is optimized for data collection from very small crystals. A long needle-shaped crystal was mounted in a nylon loop, treated with mother liquor containing 20% glycerol and vitrified in a liquid nitrogen stream at 100 K. The X-ray beam had an approximate diameter of 7 µm and a wavelength of 0.873 Å. Successive partial data sets were collected from four different spots on the same crystal.

The beamline was equipped with a MAR Mosaic 225 detector. For data collection, we used a crystal-to-detector distance of 168 mm and a total of 83 oscillation images of 1° per exposure were collected in a stream of nitrogen at 100 K. Data were processed, scaled and reduced using *XDS* (Kabsch, 1993). The crystal belongs to the trigonal system, space group $P3_121$, with unit-cell parameters $a = b = 54.23$, $c = 72.01$ Å, $\alpha = \beta = 90$, $\gamma = 120°$. There is one protein molecule in the asymmetric unit, with a crystal solvent content of 37.27%. The data set is 97.7%

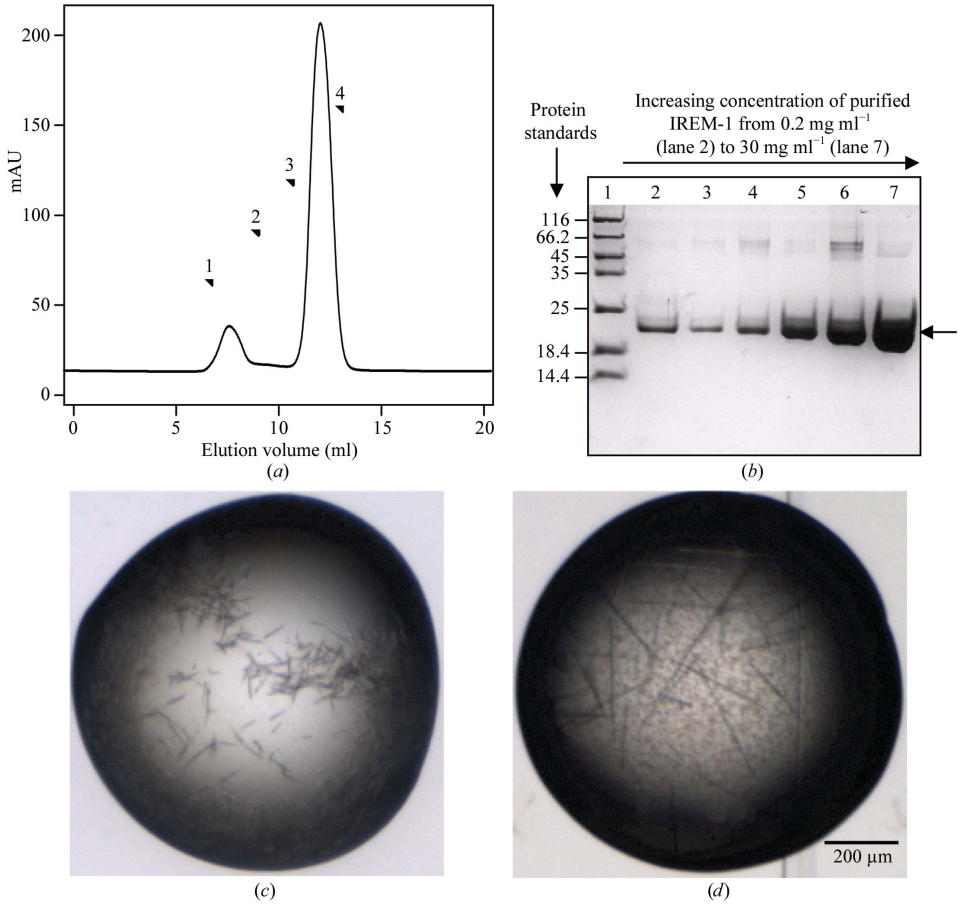

Figure 1
Protein expression, gel-filtration purification, crystallization and crystal optimization of IREM-1. (*a*) Gel-filtration chromatography of refolded and thrombin-cleaved IREM-1. This chromatography was performed at 277 K using a Superdex 75 HR 10/30 column (GE Healthcare) with a buffer containing 20 m*M* Tris–HCl pH 8.0, 150 m*M* NaCl and a flow rate of 0.5 ml min^{-1}. A low-molecular-weight gel-filtration calibration kit (GE Healthcare; Piscataway, NJ, USA) containing (1) albumin (67 000 Da), (2) ovalbumin (43 000 Da), (3) chymotrypsinogen A (25 000 Da) and (4) ribonuclease A (13 700 Da) was used as molecular-weight standards. Blue Dextran (2 000 000 Da) was used to measure the void volume of the column. This chromatography shows that IREM-1 is monomeric in solution under these experimental conditions. (*b*) SDS–PAGE under reducing conditions of purified IREM-1 at increasing concentrations. The gel was stained with colloidal Coomassie. The protein molecular-weight standards are labelled (in kDa). (*c*) Initial crystals of IREM-1 from JCSG+ condition No. 81. (*d*) IREM-1 crystals after refinement.

complete to 2.6 Å resolution. Detailed X-ray data-collection statistics are presented in Table 1.

3. Results

3.1. Cloning, protein expression and purification

The DNA encoding the extracellular immunoglobulin-like domain of IREM-1 (amino acids 21–140) was assembled *in vitro* using a recursive PCR technique. The DNA sequence was optimized for maximum protein expression by replacing low-usage codons with those preferentially used in *E. coli*. This strategy resulted in high levels of protein expression.

Recombinant expressed IREM-1 localized in inclusion bodies, with a yield of 35 mg per litre of bacterial culture. The inclusion bodies were extracted, washed extensively and solubilized in 8 *M* urea. IREM-1 protein was successful refolded by dilution using a combination of reduced and oxidized glutathione in a buffer containing a high concentration of arginine. Typically, about 25% of the initial material was recovered as correctly folded protein. The refolded protein was purified by nickel-affinity chromatography with subsequent cleavage of the histidine tag by thrombin (data not shown). After the thrombin digestion, four residues from the thrombin cleavage site were incorporated at the N-terminus of the IREM-1 sequence. The cleaved product was purified using gel-filtration chromatography. As seen in Fig. 1(*a*), the protein elutes from the gel-filtration column as a single symmetric peak, with an elution volume corresponding to the monomeric form of the protein. We attempted to further purify the protein using anion-exchange chromatography, but the protein showed a tendency to aggregate, resulting in low yields. Higher molecular-weight species were also detectable in SDS–PAGE gels (under reducing conditions) at high protein concentrations (Fig. 1*b*). To avoid this problem, we proceeded to protein concentration directly after the gel-filtration step (Fig. 1*b*).

3.2. Crystallization and crystal optimization

Initial crystallization screenings were carried out taking advantage of the high-throughput crystallization facility at the EMBL Grenoble Outstation. The protein was screened at two different initial sample concentrations, 5 and 34 mg ml^{-1}, against 768 crystallization cocktails using a total sample volume of 120 µl per concentration. Only the more concentrated sample produced crystals in a single condition containing PEG MME 2000 and potassium thiocyanate. The initial crystals were small needles of about 5 × 40 µm (Fig. 1*c*). Optimization experiments were carried out varying the concentrations of PEG and potassium thiocyanate. Crystalline material was found over a wide range of conditions, ranging from 12.5 to 37.5%(*w*/*v*) PEG MME 2000 and from 100 to 300 m*M* potassium thiocyanate; however, its quality increased only moderately compared with the initial screening, with the best crystals being long needles with approximate dimensions of 300 × 10 × 10 µm (Figs. 1*d*, 2*a*, 2*b* and 2*c*). The tendency of the protein to aggregate (see §3.1) might be a cause of the small size of the crystals obtained. Indeed, crystals were always found to co-exist with amorphous protein precipitate. This material was not suitable for routine data collection at standard synchrotron beamlines. However, successful data collection from these microcrystals was carried out using the newly operating microfocusing beamline ID23-2 of the ESRF (see later).

3.3. The microfocusing beamline ID23-2 at ESRF

It has become clear in recent years that reducing the beam size to the size of the smallest crystals while maintainng its 'brightness' can greatly enhance the quality of the diffraction by dramatically reducing the background and therefore increasing the signal-to-noise ratio. The feasibility of such an approach for macromolecular crystallography has been demonstrated in the past on ID13 at the ESRF (Cusack *et al.*, 1998). Recently, the ESRF and the EMBL have collaborated to provide and run a beamline, ID23-2, that has a beam size smaller than 10 µm in diameter while retaining the same easy-to-

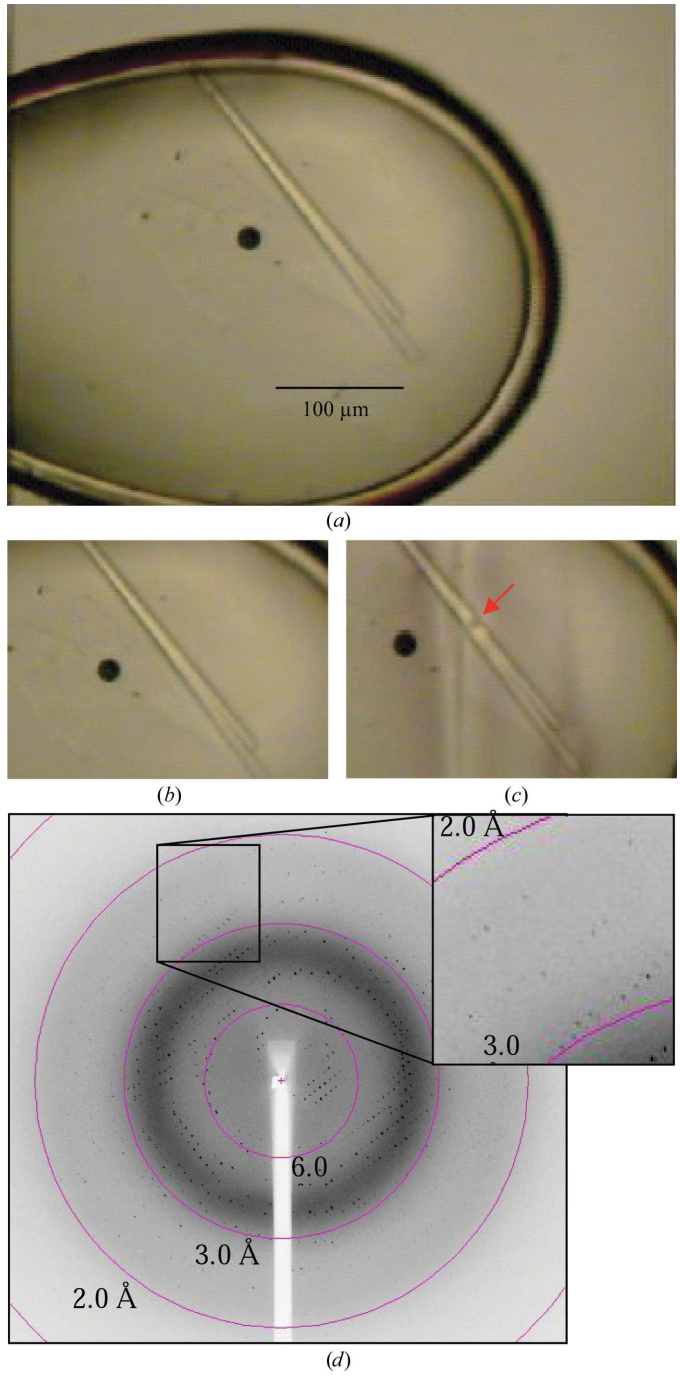

Figure 2
X-ray data collection from IREM-1 microcrystals. (*a*) IREM-1 needle crystal mounted in a nylon loop in a cryogenic stream at the ID23-2 beamline of the ESRF. Approximate crystal dimensions are 300 × 10 × 10 µm. IREM-1 crystals before (*b*) and after (*c*) exposure to the microfocused X-ray beam. The damage caused by the intense radiation, which is visible as a dark spot on the crystal indicated by a red arrow, reveals the area illuminated by the beam. (*d*) Typical diffraction frame of IREM-1.

use environment and reliability as the other ESRF MX beamlines (ID14, ID23-1 and ID29) and that is fully dedicated to macromolecular crystallography.

ID23-2 is a fixed-wavelength ($\lambda = 0.873$ Å) beamline and the X-ray beam is focused to 7.5 × 5.5 µm (horizontal × vertical FWHM) by a set of two Pt-coated Si mirrors mounted in a Kirkpatrick–Baez geometry. This allows routine collection of data on very small biological samples, the probing of several parts of a crystal larger than the beam where the crystal quality is not homogeneous or (as here) the collection of several data sets from different positions in a thin needle and minimization of the background by avoiding scattering from the cryoprotectant as the beam more or less matches the needle diameter (Fig. 2*c*). It is the first worldwide fully dedicated microfocus beamline for macromolecular crystallography.

3.4. X-ray data collection

The diffraction pattern of IREM-1 at ID23-2 (without beam attenuation) showed reflections to a resolution of 2.2 Å. However, a rapid decrease of the intensity of the reflections in the higher resolution shells was evident after a few frames, which we interpreted as an effect of radiation damage. Increased radiation damage compared with standard synchrotron beamlines is expected at ID23-2, given the high intensity of the beam and its very limited area; however, this problem was overcome by translating the crystal and collecting four independent data sets at different positions. Data-collection statistics for the four individual data sets are presented in Table 1. The final merged and scaled data set extends to 2.6 Å resolution, is 97.7% complete and has an $R_{\rm merge}$ of 14.2% (Table 1). Figs. 2(*b*) and 2(*c*) show the crystal before and after collection of the first data set, respectively. The radiation damage induced on the sample can also be appreciated as a dark spot (red arrow in Fig. 2*c*) and illustrates the relative size of the microfocus beam and the crystal. The unit-cell parameters are compatible with the presence of one molecule of IREM-1 per asymmetric unit and a solvent content of 37.27%.

We determined the three-dimensional structure of IREM-1 (Márquez *et al.*, 2007) by molecular replacement using the structural information of mouse myeloid receptor extracellular domain CLM-1 (Chung *et al.*, 2003) as a model (PDB code 1z0x), given the high percentage of identity (∼58%) between the two proteins.

This work was supported in part by the Fondazione Gerolamo Galini (Genova, Italy). We would like to thank Professor Lorenzo Moretta (Istituto Giannina Gaslini, Genova, Italy) for constant scientific support. We thank Dr Oscar Moran (Istituto di Biofisica, CNR, Genova 16149, Italy) for valuable discussion and critical reading of the manuscript. We would like to thank Elena Galfrè and Alessandro Faravelli (Istituto Giannina Gaslini, Genova, Italy) for their valuable help during protein expression and purification.

References

Aguilar, H., Alvarez-Errico, D., Garcia-Montero, A. C., Orfao, A., Sayos, J. & Lopez-Botet, M. (2004). *J. Immunol.* **173**, 6703–6711.
Allcock, R. J., Barrow, A. D., Forbes, S., Beck, S. & Trowsdale, J. (2003). *Eur. J. Immunol.* **33**, 567–577.
Alvarez-Errico, D., Aguilar, H., Kitzig, F., Brckalo, T., Sayos, J. & Lopez-Botet, M. (2004). *Eur. J. Immunol.* **34**, 3690–3701.
Berg, T. K. van den, Yoder, J. A. & Litman, G. W. (2004). *Trends Immunol.* **1**, 11–16.
Bouchon, A., Dietrich, J. & Colonna, M. (2000). *J. Immunol.* **164**, 4991–4995.
Cantoni, C., Bottino, C., Augugliaro, R., Morelli, L., Marcenaro, E., Castriconi, R., Vitale, M., Pende, D., Sivori, S., Millo, R., Biassoni, R., Moretta, L. & Moretta, A. (1999). *Eur. J. Immunol.* **10**, 3148–3159.
Chung, D. H., Humphrey, M. B., Nakamura, M. C., Ginzinger, D. G., Seaman, W. E. & Daws, M. R. (2003). *J. Immunol.* **171**, 6541–6658.
Clark, G. J., Green, B. J. & Hart, D. N. (2000). *Tissue Antigens*, **55**, 101–109.
Colonna, M., Navarro, F., Bellon, T., Llano, M., Garcia, P., Samaridis, J., Angman, L., Cella, M. & Lopez-Botet, M. (1997). *J. Exp. Med.* **186**, 1809–1818.
Cusack, S., Belrhali, H., Bram, A., Burghammer, M., Perrakis, A. & Riekel, C. (1998). *Nature Struct. Biol.* **5**, 634–637.
Dietrich, J., Nakajima, H. & Colonna, M. (2000). *Microbes Infect.* **3**, 323–329.
Dimasi, N. & Biassoni, R. (2005). *Immunol. Cell Biol.* **83**, 1–8.
Dimasi, N., Roessle, M., Moran, O., Candiano, G., Svergun, D. I. & Biassoni, R. (2007). *Int. J. Biol. Macromol.* **40**, 193–200.
Fujioka, Y., Matozaki, T., Noguchi, T., Iwamatsu, A., Yamao, T., Takahashi, N., Tsuda, M., Takada, T. & Kasuga, M. (1996). *Mol. Cell. Biol.* **12**, 6887–6899.
Green, B. J., Clark, G. J. & Hart, D. N. (1998). *Int. Immunol.* **10**, 891–899.
Humphrey, M. B., Lanier, L. L. & Nakamura, M. C. (2005). *Immunol. Rev.* **208**, 50–65.
Kabsch, W. (1993). *J. Appl. Cryst.* **26**, 795–800.
Márquez, J. A., Galfre, E., Dupeux, F., Flot, D., Moran, O. & Dimasi, N. (2007). In the press.
Martinez-Barriocanal, A. & Sayos, J. (2006). *J. Immunol.* **177**, 2819–2830.
Natarajan, K., Dimasi, N., Wang, J., Mariuzza, R. A. & Margulies, D. H. (2002). *Annu. Rev. Immunol.* **20**, 853–885.
Pandey, S. & Agrawal, D. K. (2006). *Immunol. Cell Biol.* **84**, 333–341.
Ravetch, J. V. & Lanier, L. L. (2000). *Science*, **290**, 84–89.
Speckman, R. A., Wright Daw, J. A., Helms, C., Duan, S., Cao, L., Taillon-Miller, P., Kwok, P. Y., Menter, A. & Bowcock, A. M. (2003). *Hum. Genet.* **112**, 34–41.